

# Blackbox Quantization of Superconducting Circuits using exact Impedance Synthesis

Firat Solgun<sup>1,2</sup>, David W. Abraham<sup>3</sup>, and David P. DiVincenzo<sup>1,2,4</sup>

<sup>1</sup> Institute for Quantum Information, RWTH Aachen, Germany

<sup>2</sup> Jülich-Aachen Research Alliance (JARA), Fundamentals of Future Information Technologies, Germany

<sup>3</sup> IBM T.J. Watson Research Center, Yorktown Heights, NY 10598, USA and

<sup>4</sup> Peter Grünberg Institute: Theoretical Nanoelectronics, Research Center Jülich, Germany

We propose a new quantization method for superconducting electronic circuits involving a Josephson junction device coupled to a linear microwave environment. The method is based on an exact impedance synthesis of the microwave environment considered as a blackbox with impedance function  $Z(s)$ . The synthesized circuit captures dissipative dynamics of the system with resistors coupled to the reactive part of the circuit in a non-trivial way. We quantize the circuit and compute relaxation rates following previous formalisms for lumped element circuit quantization. Up to the errors in the fit our method gives an exact description of the system and its losses.

The increase in  $Q$ -factors of superconducting qubits and cavities requires highly accurate models for their design, optimization and predictability. The common approach to model such systems has been to use Jaynes-Cummings type Hamiltonians borrowed from quantum optics. However several problems arise like convergence issues when one wants to include higher levels of superconducting qubits or higher modes of cavities in such models [1].

To remedy those issues a method is proposed in [2] to derive Hamiltonians and compute relaxation rates for superconducting circuits. In this method the linear electromagnetic environment shunting the Josephson junction, as extracted, for example, using microwave simulation software, is lumped together with the junction's linear inductance, to give a "blackbox" impedance function  $Z_{sim}(\omega)$ . This response is then fitted, pole by pole, to an analytic function  $Z(\omega)$ . Then an approximate version of Foster's theorem [3] in the low loss limit [4], applied to  $Z(\omega)$ , gives an equivalent circuit as a series connection of resonant  $RLC$  stages, one stage for each term in the partial fraction expansion of  $Z(\omega)$ . In this method, which we refer to as the "lossy Foster" method,  $Q$  factors for each resonant mode are computed using  $Q_p = \frac{\omega_p \text{Im}[Y'(\omega_p)]}{2 \text{Re}[Y(\omega_p)]}$  where  $\omega_p = (L_p C_p)^{-1}$  and  $Y = Z^{-1}$ . The lifetime of the mode is given by  $T_p = Q_p / \omega_p$ .

Lossy Foster, while simple to apply, is not always accurate or even well-conditioned. Terms in the partial-fraction expansion of  $Z(\omega)$  do not always correspond to stages of a physical circuit [5]. As Brune showed [6], the property that an impedance function must have to correspond to a passive physical network is termed "PR (Positive-Real)" this property is an important theme of the present paper. We note that even if all terms in the expansion of  $Z(\omega)$  are individually  $PR$ , one might still need to remove terms by inspection to get a better fit, making the method dependent on ad-hoc decisions. As applied in [2], lossy Foster parameters are dependent not only on the properties of the electromagnetic environment, but also on the precise value of the junction inductance.

In this paper we propose a new method to derive, from

first principles, the Hamiltonian of a system consisting of a single Josephson junction connected to a linear microwave environment. As in [2], we will focus on the example involving a transmon qubit coupled to a 3D microwave cavity. We also treat the electromagnetic environment that the junction sees as a black box with an impedance  $Z_{sim}$ . To get  $Z_{sim}$  we first simulate the cavity system (not including the linear part of the Josephson inductance) and fit the numerical impedance response to a rational function  $Z(s)$

$$Z(s) = \frac{n(s)}{d(s)} = \sum_k \frac{R_k}{s - s_k} + d + es \quad (1)$$

(here  $s$  is the Laplace variable) using a well established technique [7]. We then apply the formalism discovered by Brune [6] to synthesize a circuit that has *exactly* the impedance  $Z(s)$  across its terminals. We call the synthesized circuit the "Brune circuit". Since the Brune circuit has a non-trivial topology, we resort to [8, 9] to derive its Hamiltonian and compute relaxation rates. Our method, unlike the previous lossy Foster approach [2], involves no approximation in circuit synthesis. Hence the accuracy of our Hamiltonian and dissipation analysis give an exact description except for very small errors, introduced in fitting, which are inevitable in both approaches.

After obtaining the rational function fit Eq. (1) to  $Z(s)$  (details of which are described below), we use results from electrical circuit synthesis theory to obtain a lumped element circuit having exactly this impedance. Brune [6] showed that any impedance response  $Z(s)$  satisfying the  $PR$  conditions can be realised with a finite electric circuit. He gave an algorithm to find such a lumped element circuit admitting the  $PR$  impedance function  $Z(s)$ . This extends Foster's original work [3], which applies only to lossless networks. For details of Brune's algorithm see [10], Sec. III.B; see also [5]. Applying Brune's algorithm to  $Z(s)$  gives a lumped circuit of the form shown in Fig. 1.

Brune's circuit consists of  $M$  stages each containing a tightly-coupled inductor pair ( $M_j = \sqrt{L_{j1} L_{j2}}$ ), a capacitor  $C_j$ , and a series resistor  $R_j$ . As shown below, this interleaving of  $M$  lossless stages with  $(M + 1)$  resistors

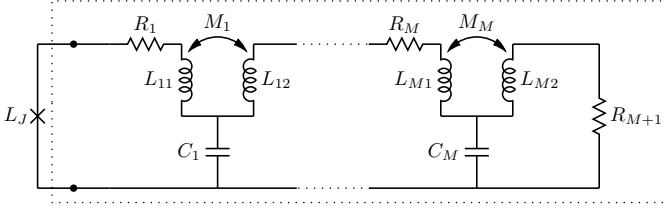


Figure 1: Brune circuit (in dotted box) shunted by a Josephson junction. The analysis of this circuit is extensively discussed in [10], Secs. II and III.

results in non-trivial coupling between modes of the circuit and the dissipative environment represented by these resistors.

We quantize the Brune circuit following the formalism of [9]. For the Caldeira-Leggett treatment of resistors we refer to [8]. Here we present results of the derivation in [10], Sec. II; we find a Lagrangian  $\mathcal{L}_S$  (or equivalently a Hamiltonian  $\mathcal{H}_S$ ) corresponding to a 1D chain of interacting oscillator degrees of freedom:

$$\mathcal{L}_S = \frac{1}{2} \dot{\Phi}^T \mathcal{C} \dot{\Phi} - U(\Phi), \mathcal{H}_S = \frac{1}{2} \mathbf{Q}^T \mathcal{C}^{-1} \mathbf{Q} + U(\Phi), \quad (2)$$

where

$$U(\Phi) = - \left( \frac{\Phi_0}{2\pi} \right)^2 L_J^{-1} \cos(\varphi_J) + \frac{1}{2} \Phi^T \mathbf{M}_0 \Phi. \quad (3)$$

Here  $\Phi$  is a vector of length  $(M+1)$  whose entries are linear combinations of branch fluxes in the Brune circuit (see [10] Eqs. (18,19) for details). The Josephson phase  $\varphi_J$  is not an independent coordinate, but it is given in terms of the variables in the vector  $\Phi$  by  $(\Phi_0/2\pi)\varphi_J = \sum_j (-1)^{j+1} \Phi_j$ . The chain structure of our representation is evident in the tri-diagonality of the capacitance and inverse inductance matrices:

$$\mathcal{C} = \begin{pmatrix} C'_1 & t_1 C'_1 & & & 0 \\ t_1 C'_1 & t_1^2 C'_1 + C'_2 & \ddots & & \\ & \ddots & \ddots & & \\ 0 & & & t_{M-1}^2 C'_{M-1} + C'_M & t_M C'_M \\ & & & t_M C'_M & t_M^2 C'_M \end{pmatrix}, \quad (4)$$

$$\mathbf{M}_0 = \begin{pmatrix} \frac{1}{L'_1} & \frac{1}{L'_1} & & & 0 \\ \frac{1}{L'_1} & \frac{1}{L'_1} + \frac{1}{L'_2} & \ddots & & \\ & \ddots & \ddots & & \\ 0 & & & \frac{1}{L'_{M-1}} + \frac{1}{L'_M} & \frac{1}{L'_M} \\ & & & \frac{1}{L'_M} & \frac{1}{L'_M} \end{pmatrix}, \quad (5)$$

$C'_j = C_j / (1 - t_j)^2$ ,  $L'_j = L_{j2} (1 - t_j)^2$  and  $t_j = \sqrt{\frac{L_{j1}}{L_{j2}}}$ .

Applying Eq. (124) of [8] we get the contribution to the relaxation rate from the resistor  $R_j$  ( $1 \leq j \leq M+1$ ):

$$\frac{1}{T_{1,j}} = 4 |\langle 0 | \bar{\mathbf{m}}_j \cdot \Phi | 1 \rangle|^2 J_j(\omega_{01}) \coth \left( \frac{\hbar \omega_{01}}{2k_B T} \right) \quad (6)$$

$k$	Pole $s_k$ (GHz)	Residue $R_k$
1	$-1.6152 \times 10^{-6}$	8363.13
2,3	$-0.00110372 \pm j6.87473$	$5.69612 \pm j0.00369273$
4,5	$-0.00671733 \pm j7.05711$	$(6.26609 \pm j1.34164) \times 10^{-5}$
6,7	$-1.34901 \pm j8.98453$	$(7.33283 \pm j5.61551) \times 10^{-3}$
8,9	$-0.00272701 \pm j12.0048$	$7.15159 \pm j0.0227882$
10,11	$-0.00918635 \pm j12.8561$	$(1.98602 \pm j0.0134996) \times 10^{-3}$
12,13	$-1.40214 \pm j13.7644$	$(-8.60807 \pm j9.40397) \times 10^{-3}$
14,15	$-0.131778 \pm j17.7404$	$23.8075 \pm j1.17404$
16,17	$-3.14927 \pm 88.3524j$	$(1.19527 \pm j0.120033) \times 10^4$

Table I: Poles and residues for the fit to the HFSS dataset for  $Z_{sim}$  as in the second part of Eq. (1).

$|0, 1\rangle$  are the qubit eigenlevels of the system Hamiltonian Eq. (2). The vector  $\bar{\mathbf{m}}_j$  (of length  $(M+1)$ ) describes the coupling of the system to the environment representing resistor  $R_j$ ; for our Brune circuit this is, for  $1 \leq j \leq M$ :

$$\bar{\mathbf{m}}_j = \begin{pmatrix} 0 \\ \vdots \\ 0 \\ \frac{(-1)^{j-1} C_j}{(1-t_j)} \\ \frac{(-1)^j C_{j+1}}{(1-t_{j+1})} + \frac{(-1)^{j-1} t_j C_j}{(1-t_j)} \\ \vdots \\ \frac{(-1)^{M-1} C_M}{(1-t_M)} + \frac{(-1)^{M-2} t_{M-1} C_{M-1}}{(1-t_{M-1})} \\ \frac{(-1)^{M-1} t_M C_M}{(1-t_M)} \end{pmatrix}. \quad (7)$$

The spectral density corresponding to the bath representing  $R_j$  is

$$J_j(\omega) = \omega^3 R_j \left[ 1 + \omega^2 R_j^2 \left( \sum_{k=j}^M C_k \right)^2 \right]^{-1}. \quad (8)$$

For the last resistor  $R_{M+1}$ ,  $\bar{\mathbf{m}}_{M+1} = (0 \cdots 0 \ 1)^T$  and  $J_{M+1}(\omega) = \omega / R_{M+1}$ .

To show the application of the synthesis method we have just described, we analyse a dataset produced to analyse a recent 3D transmon experiment at IBM [11]. Our modeling is performed using the finite-element electromagnetics simulator HFSS[12]. Since the systems we want to model admit very small loss [13, 14], they are very close to the border which separates stable (passive) systems from unstable ones. Therefore it is necessary to take care that the simulation resolution is high enough to ensure the passivity of the simulated impedance. Otherwise the fitted impedance  $Z(s)$  does not satisfy the *PR* conditions [6] meaning that there is no passive physical network corresponding to  $Z(s)$ .

The physical device that is modelled using HFSS is a rectangular cavity with a transmon qubit mounted in its center (see [10], Figs. 1 and 2). The simulation includes

two coaxial ports entering the body of the cavity symmetrically on either side of the qubit. HFSS is used to calculate the device’s three-port  $S$  matrix over a wide frequency range, from 3.0 to 15.0 GHz. The three ports are those defined by the two coaxial connectors and the qubit terminal pair. That is, the metal defining the Josephson junction itself is absent from the simulation, so that its capacitance and (nonlinear) inductance can be added back later as a discrete element as in Fig. 1. The conversion from the  $S$  matrix to  $Z_{sim}$  is calculated using standard formulas [15, 16], in which it is assumed that the two coaxial ports are terminated with a matched ( $Z_0=50\Omega$ ) resistor. We have confirmed that the lossy part of the resulting impedance is mostly determined by these port terminations, rather than by the (physically rather inaccurate) HFSS model of cavity-metal losses; this is consistent with the  $Q$  of the system being determined by its external couplings [11].

To obtain the fitted rational impedance function  $Z(s)$  as in Eq. (1), we use the MATLAB package Vector Fitting [7]. Vector Fitting is an algorithm to approximate a sampled impedance/admittance response by a rational function. It takes a dataset over sampled frequency points, and the number of poles required for the fit, as its input and gives a set of poles and residues as its output (See [17] for models with infinite number of poles). Ref. [18] discusses details of Vector Fitting. Its passivity enforcement subroutine [19] makes sure that the real part of the resulting rational approximation is positive definite. This feature is crucial for our analysis since we require the impedance response to be PR (see [10], Sec. IIIA) for the existence of a finite passive network having the same impedance across its terminals. Note that passivity enforcement may not always work if the accuracy of the microwave simulation is not high enough and we have taken care to run the simulation with suitably high resolution. Applying Vector Fitting to  $Z_{sim}$  gives the partial fraction expansion form in Eq. (1) with the poles  $s_k$  and residues  $R_k$  listed in Table I, with  $e = 0$  and  $d = 2.80407\Omega$ . Note that some of the poles obtained in the fit have frequencies (imaginary part of  $s_k$ ) outside the range of the simulation data; this is a normal feature of the fitting routine, used to guarantee a highly accurate fit throughout the entire simulated frequency band.

We have applied both Brune’s algorithm and a lossy Foster analysis to our fitted  $Z(s)$ . Circuit parameters obtained for the Brune circuit are listed in Table II. We see that the series resistor connected directly to the qubit is quite tiny – the qubit is nearly lossless. The progressive increase of the resistance values in further stages of the circuit does not imply a large contribution of these resistors to loss, as they are seen by the qubit only through a kind of  $LC$  “filter”. Indeed, the strong trend towards increasing impedance from stage to stage in the Brune network (both in the  $R$  and  $\sqrt{L/C}$  values) means that the first few stages of the Brune network already give a good approximation of the cavity response  $Z(s)$ .

$i$	$R_i (\Omega)$	$C_i (nF)$	$L_{i1} (nH)$	$L_{i2} (nH)$
1	$5.71974 \times 10^{-5}$	$1.17020 \times 10^{-4}$	$1.32810 \times 10^{-1}$	$3.02058 \times 10^1$
2	$5.53199 \times 10^{-2}$	$2.49081 \times 10^{-6}$	$8.75272 \times 10^1$	$3.74225 \times 10^3$
3	$1.84087 \times 10^2$	$6.01727 \times 10^{-8}$	$4.12954 \times 10^3$	$1.98121 \times 10^4$
4	$1.79021 \times 10^4$	$1.44153 \times 10^{-9}$	$4.56024 \times 10^4$	$2.67489 \times 10^5$
5*	$6.57108 \times 10^5$	$2.01906 \times 10^{-10}$	0	0
6	$4.90091 \times 10^5$	$9.69933 \times 10^{-12}$	$1.56173 \times 10^7$	$1.55436 \times 10^7$
7	$4.14678 \times 10^7$	$1.64015 \times 10^{-12}$	$3.09821 \times 10^8$	$3.1134 \times 10^8$
8	$2.33793 \times 10^7$	$6.32007 \times 10^{-11}$	$4.74168 \times 10^6$	$1.95174 \times 10^6$
9	$1.22342 \times 10^8$	$1.70536 \times 10^{-11}$	$7.42302 \times 10^6$	$1.10608 \times 10^7$

$$R_{10} = 6.35712 \times 10^8 \Omega$$

Table II: Parameter values for synthesized Brune circuit. Note the strong (orders of magnitude) increase in impedance (in  $R$  and  $\sqrt{L/C}$  values) as we go deep in the circuit. 5<sup>th</sup> stage is degenerate treated in more detail in [10], Sec. II.A.

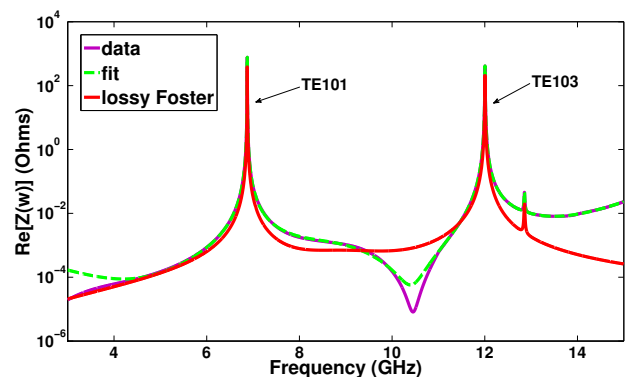


Figure 2: Real part of open-circuit response. Dotted green is open-circuit response for the Brune circuit which we identify with the open-circuit fit. Solid magenta is the simulated response. Red is the response of lossy Foster circuit.  $TE101$  and  $TE103$  are the resonances associated with classical rectangular cavity modes[20].

In fitting our data with the lossy Foster method (see [10]) one must be careful about residues with negative real parts or significant imaginary parts. Note that one cannot apply the lossy Foster approximation to terms corresponding to poles 12 and 13 in Table I since they have residues with negative real parts — there is no physical network to approximate those terms alone. We also drop DC and high-frequency terms corresponding to poles 1 and 14 – 17 respectively: such a choice gives a better approximation for the real part of the impedance in the frequency band of interest. Thus, the best approximating Foster network consists of five RLC stages, representing the ten remaining pole pairs.

In Fig. 2 we compare these open-circuit impedances, as represented by the Brune and lossy-Foster methods, over the full range of our simulation data. The Foster representation clearly captures the main features of the response, notably the two classical box resonances of the

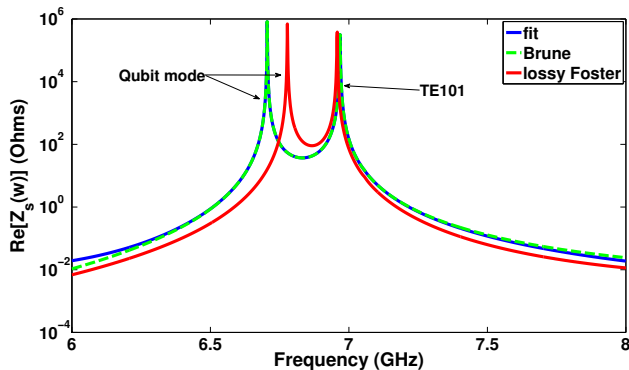


Figure 3: Real part of impedance in a small range of frequencies around the qubit pole ( $f_{qb} = 6.7052$  GHz where  $f_{qb}$  is the qubit resonance for the exact fit) for the system shunted (with impedance  $Z_s$ ) by a linear inductance  $L_J = 4.5$  nH representing the Josephson junction for three different cases. The  $TE101$  mode is not strongly affected by the presence of  $L_J$ .

cavity. But in finer details, especially far away from the resonances, the Brune representation, which is essentially indistinguishable from the fit obtained from Vector Fitting, matches much better than the best lossy Foster circuit.

We now show the improvements that can be expected by using the Brune circuit when representing the dynamics of the qubit-cavity system. Here we perform only simple calculations involving a harmonic qubit (i.e., one represented by a linear inductance  $L_J$ ), but our results give evidence that the Brune circuit will provide high-quality predictions even for more complex, strongly anharmonic qubits. In Fig. 3 we show the lossy part of the impedance when the cavity is shunted by a linear inductance  $L_J = 4.5$  nH. The fundamental cavity resonance ( $TE101$ ) is not significantly changed from the open circuit case, but the qubit appears as a new pole in the response. This “qubit pole” is again very accurately represented by the Brune circuit; however, using the lossy-Foster circuit derived from the open circuit case above, the qubit pole is significantly misplaced, by about 100MHz.

Of course, in current applications of the Foster approach [2], one can do much better by refitting the Foster form with the linear inductance included in the response, and thus adding a new RLC stage to explicitly represent the qubit pole. This is an effective strategy, but the results in Fig. 4 indicate its limitations.

Here we compare the use of the Brune and (fixed) lossy-Foster circuit in giving the real part of the qubit

pole, which is proportional to the relaxation rate  $1/T_1$  Eq. (6), as the inductance  $L_J$  is varied. We see again that the Brune circuit matches the “fit” result, obtained directly from the HFSS data, very closely. The deviations of the lossy-Foster result are up to 20%, and the decrease of the loss rate with  $L_J$  is significantly underestimated.

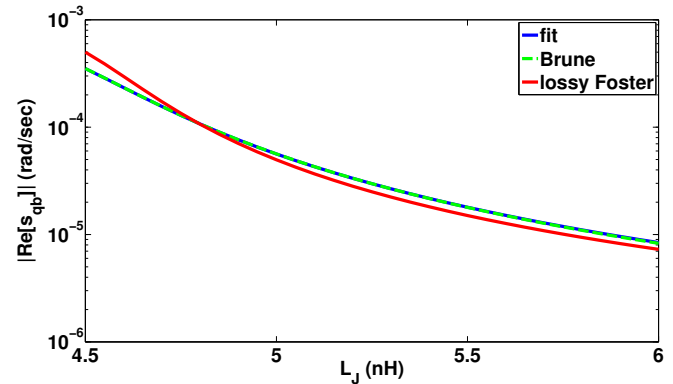


Figure 4: Magnitude of the real part of qubit pole  $s_{qb}$  as a function of linear inductance representing the Josephson junction shunting the system for three different cases: exact fit for the system shunted by the linear inductance, Brune circuit shunted by the linear inductance and lossy Foster circuit shunted by the linear inductance.  $T_1$  relaxation rate of the qubit is given by  $T_1^{-1} = \omega_{qb}/Q_{qb}$ , where the quality factor  $Q_{qb} = \omega_{qb}/|\xi_{qb}|$  with  $\xi_{qb} = Re[s_{qb}]$ , and  $\omega_{qb} = Im[s_{qb}]$  is the frequency of the qubit mode.

This suggest that no single lossy-Foster network, incorporating some fixed amount of linear inductance, will be able to match this trend.

Thus, while the Foster approach has been of considerable value in modelling nearly harmonic qubits like transmons [2], it appears that the exactness of the Brune approach will be of real value as we consider other, more anharmonic cavity-coupled qubits. A clear application in this direction will be the cases of fluxonium [21] or flux qubits [22] – our approach should provide a highly accurate multi-mode Hamiltonian for modelling dynamics in those cases. As we move also to multi-qubit, multi-port modelling problems, we are hopeful that application of further electrical theories, developed actively for problems of network synthesis in the decades after Brune’s work, will prove very useful in providing new modelling techniques for contemporary quantum computer devices.

We thank Gianluigi Catelani for a critical reading of this manuscript. We are grateful for support from the Alexander von Humboldt foundation.

[1] Jerome Bourassa, Jay M. Gambetta, and Alexandre Blais, “Multi-mode circuit quantum electrodynamics,” Abstract Y29.00005, APS March Meeting, Dallas, 2011.

[2] S. E. Nigg, H. Paik, B. Vlastakis, G. Kirchmair, S. Shankar, L. Frunzio, M. H. Devoret, R. J. Schoelkopf, and S. M. Girvin, “Black-Box Superconducting Circuit

- Quantization”, Phys. Rev. Lett. 108, 240502 (2012).
- [3] Foster, R. M., “A reactance theorem”, Bell Systems Technical Journal, vol.3, no. 2, pp. 259–267, November 1924.
- [4] E. R. Beringer, “Resonant Cavities as Microwave Circuit Elements,” in *Principles of Microwave Circuits*, edited by C. G. Montgomery, R. H. Dicke, and E. M. Purcell (MIT Radiation Laboratory, vol. 8, 1945), p. 215, Section 7.4.
- [5] Ernst A. Guillemin, *Synthesis of Passive Networks*, (Robert E. Krieger Publishing Company, Huntington, New York, 1977), Chap. 9.
- [6] O. Brune, *Synthesis of a finite two-terminal network whose driving-point impedance is a prescribed function of frequency*, Doctoral thesis, MIT, 1931.
- [7] B. Gustavsen and A. Semlyen, "Rational approximation of frequency domain responses by vector fitting", IEEE Trans. Power Delivery, vol. 14, no. 3, pp. 1052-1061, July 1999; <http://www.sintef.no/Projectweb/VECTFIT/>.
- [8] G. Burkard, R. H. Koch, and D. P. DiVincenzo, “Multi-level quantum description of decoherence in superconducting qubits”, Phys. Rev. B 69, 064503 (2004).
- [9] G. Burkard, “Circuit theory for decoherence in superconducting charge qubits”, Phys. Rev. B 71, 144511 (2005).
- [10] Supplementary Material.
- [11] Chad Rigetti, Jay M. Gambetta, Stefano Poletto, B. L. T. Plourde, Jerry M. Chow, A. D. Corcoles, John A. Smolin, Seth T. Merkel, J. R. Rozen, George A. Keefe, Mary B. Rothwell, Mark B. Ketchen, and M. Steffen, “Superconducting qubit in a waveguide cavity with a coherence time approaching 0.1 ms”, Phys. Rev. B 86, 100506(R) (2012).
- [12] Ansys HFSS (High Frequency Structural Simulator), <http://www.ansys.com>.
- [13] H. Paik, D. I. Schuster, L. S. Bishop, G. Kirchmair, G. Catelani, A. P. Sears, B. R. Johnson, M. J. Reagor, L. Frunzio, L. I. Glazman, S. M. Girvin, M. H. Devoret, and R. J. Schoelkopf, “Observation of high coherence in Josephson junction qubits measured in a three-dimensional circuit QED architecture”, Phys. Rev. Lett. 107, 240501 (2011).
- [14] M. Reagor, Hanhee Paik, G. Catelani, L. Sun, C. Axline, E. Holland, I.M. Pop, N.A. Masluk, T. Brecht, L. Frunzio, M.H. Devoret, L.I. Glazman, R.J. Schoelkopf, “Reaching 10 ms single photon lifetimes for superconducting aluminum cavities”, Appl. Phys. Lett. 102, 192604 (2013).
- [15] Robert W. Newcomb, *Linear Multiport Synthesis*, McGraw-Hill Book Company, 1966.
- [16] D. Pozar, *Microwave Engineering*, John Wiley & Sons, Inc., 2005.
- [17] M. K. Zinn, “Network Representation of Transcendental Impedance Functions”, Bell System Technical Journal 31, 378 (1951).
- [18] W. Hendrickx, and T. Dhaene, “A discussion of rational approximation of frequency domain responses by vector fitting”, IEEE Trans. Power Systems, vol. 21, no. 1, pp. 441-443, Feb. 2006.
- [19] B. Gustavsen and A. Semlyen, "Enforcing passivity for admittance matrices approximated by rational functions", IEEE Trans. Power Systems, vol. 16, no. 1, pp. 97-104, Feb. 2001.
- [20] S. Ramo, J. R. Whinnery and T. V. Duzer, *Fields and Waves in Communication Electronics*, John Wiley & Sons, Inc., 1967.
- [21] Ioan M. Pop, Kurtis Geerlings, Gianluigi Catelani, Robert J. Schoelkopf, Leonid I. Glazman, and Michel H. Devoret, “Coherent suppression of electromagnetic dissipation due to superconducting quasiparticles,” to be published.
- [22] M. Stern, Y. Kubo, C. Grezes, A. Bienfait, D. Vion, D. Esteve and P. Bertet, “Flux Qubits in Three-Dimensional Circuit-QED Architecture”, arXiv:1403.3871.
-

# Supplementary Material for "Blackbox Quantization of Superconducting Circuits using exact Impedance Synthesis"

Firat Solgun<sup>1,2</sup>, David W. Abraham<sup>3</sup>, and David P. DiVincenzo<sup>1,2,4</sup>

<sup>1</sup> *Institute for Quantum Information, RWTH Aachen, Germany*

<sup>2</sup> *Jülich-Aachen Research Alliance (JARA), Fundamentals of Future Information Technologies, Germany*

<sup>3</sup> *IBM T.J. Watson Research Center, Yorktown Heights, NY 10598, USA*

<sup>4</sup> *Peter Grünberg Institute: Theoretical Nanoelectronics, Research Center Jülich, Germany*

In these notes we present details of the HFSS simulation, a full derivation (based on the formalism in [8, 9]) of the Brune circuit Hamiltonian and relaxation rate expressions. We also discuss the definition of PR (Positive-Real) functions, Brune’s algorithm and the “lossy Foster” method in detail.

## I. DEVICE SIMULATION

The simulated device is a 3D transmon, inserted with appropriate antenna structures into the middle of a rectangular superconducting (aluminium) box cavity, which is standard in several labs presently for high-coherence qubit experiments. Fig. 5 shows a perspective rendering of the device, and Fig. 6 shows an intensity map of the fundamental mode of the cavity.

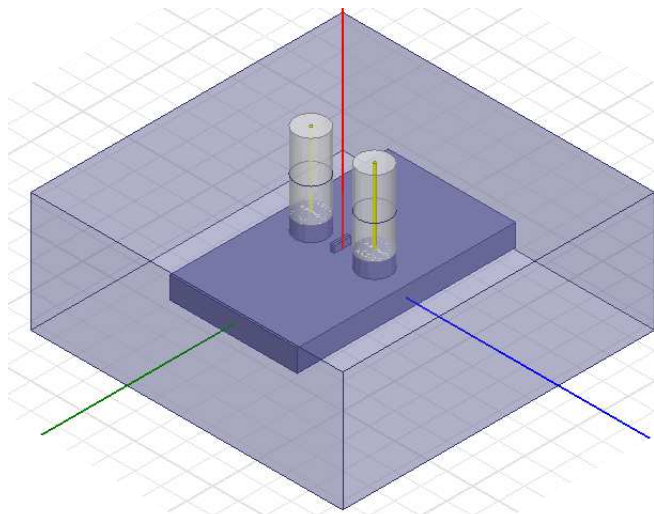


Figure 5: Geometry of the 3D transmon qubit simulated in HFSS. Light blue is perfect conductor and dark blue is the vacuum. The qubit port terminals are defined on a dielectric substrate located at the position of the red line. Two coaxial ports are positioned symmetrically on each side of the substrate. The cavity dimensions are (*height, length, width*) = (4.2mm, 24.5mm, 42mm).

## II. QUANTIZATION OF THE BRUNE CIRCUIT

An augmented form of the Brune circuit is shown in Fig. 7. The last resistor  $R_{M+1}$  is replaced with a capacitor  $C_{M+1}$ . It will be included in our analysis later through the substitution  $C_{M+1} \leftarrow 1/(i\omega R_{M+1})$ . We will compute its dissipative effect referring to the equation of motion Eq. (61) in [8]. We also add a formal capacitance  $C_J$  shunting the Josephson junction. This is required for a non-singular capacitance matrix if there are no degenerate stages (see Section (III)). Coupled inductors in the circuit in Fig. 7 satisfy “tight” coupling condition  $M_j = \sqrt{L_{j1}L_{j2}}$ . The inductance matrix  $L_t$  in Eq. (15) of [9] becomes singular in the tight coupling limit. To remedy this issue we will rotate coordinates to eliminate half of degrees of freedom corresponding to coupled inductor branches. With the ordering  $(L_J, L_{12}, L_{22}, \dots, L_{M2}, L_{11}, L_{21}, \dots, L_{M1}, R_1, \dots, R_M)$  and  $(C_J, C_1, \dots, C_M, C_{M+1})$  for tree and chord

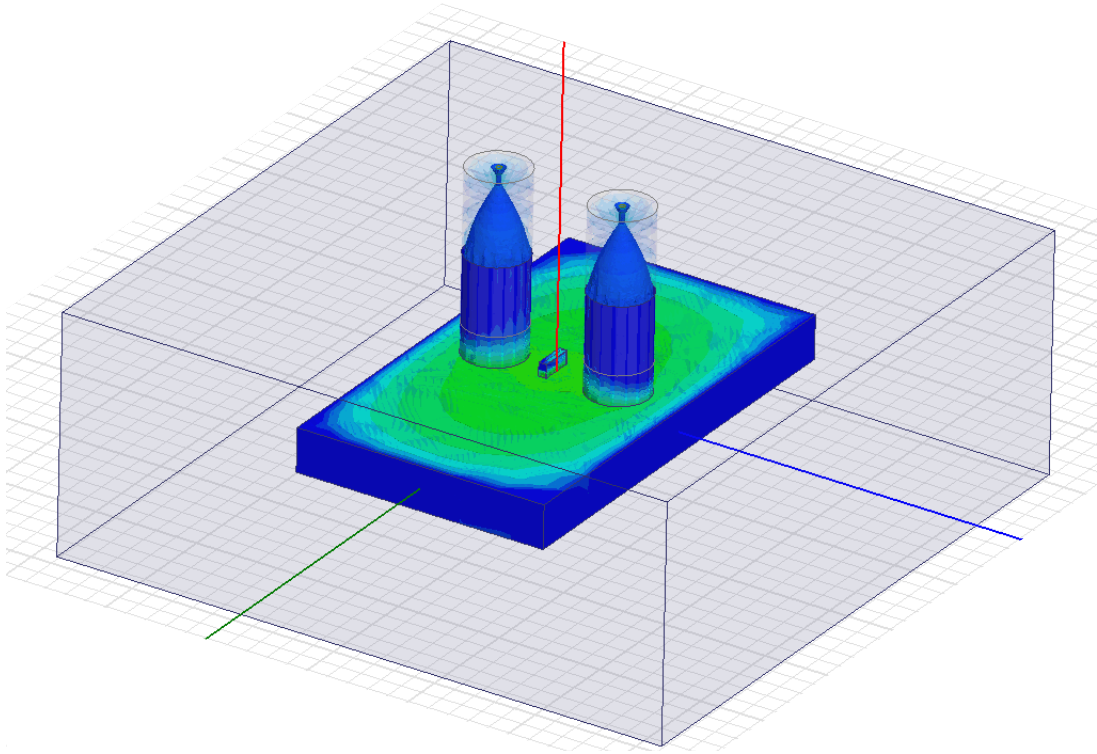


Figure 6: Fundamental mode (the  $TE_{101}$  mode) of the cavity with frequency  $f_{TE_{101}} = 6.875GHz$ . Green color indicates electric field regions of higher magnitude compared to blue regions.

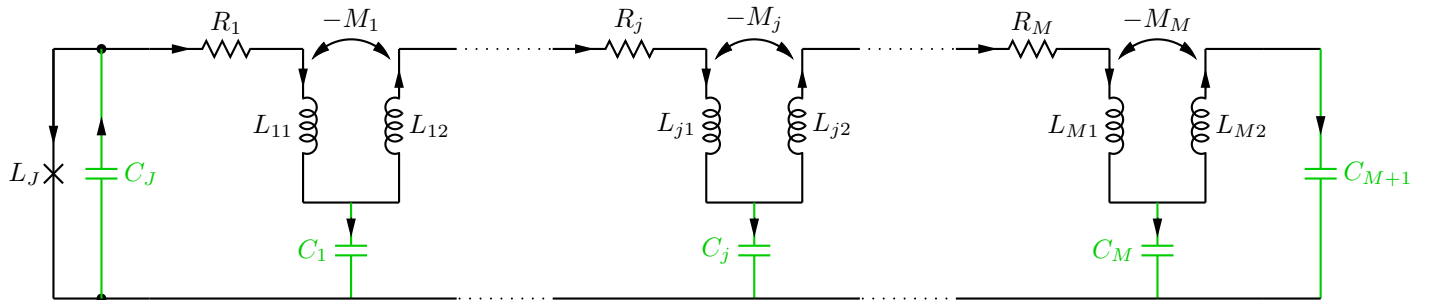


Figure 7: Modified Brune circuit. Tree branches are shown in black and chord branches are shown in green. Current directions are chosen to have the matrix  $\mathcal{F}_C$  in Eq. (9) with all positive entries.

branches respectively (note that right transformer branches come first and that there are no chord inductors), we construct  $\mathcal{F}_C$  matrix in Eq. (21) of [9] (To get  $\mathcal{F}_C$  with all positive entries we reversed the direction of currents through and inverted the polarity of voltages across right coupled inductor branches which requires the update  $M_j \rightarrow -M_j$  for mutual inductances. See Fig. 7 for directions of branch currents and Section (III) for the definition of the coupled inductor.)

$$\mathcal{F}_C = \begin{pmatrix} 1 & 1 & 1 & \cdots & 1 & 1 \\ & & 1 & \cdots & 1 & 1 \\ & & & \ddots & \vdots & \vdots \\ & 0 & & & 1 & 1 \\ & & & & & 1 \\ 0 & 1 & 1 & \cdots & 1 & 1 \\ & & 1 & \cdots & 1 & 1 \\ & & & \ddots & \vdots & \vdots \\ & 0 & & & 1 & 1 \end{pmatrix} \quad (9)$$

where  $\mathcal{F}_C$  is a  $(2M+1) \times (M+2)$  matrix. We then compute the capacitance matrix in Eq. (22) of [9] as

$$C_0 = \mathcal{F}_C C \mathcal{F}_C^t \quad (10)$$

where  $C$  is the diagonal matrix with capacitances  $(C_J, C_1, \dots, C_M, C_{M+1})$  in the diagonal. With the directions chosen for coupled inductor currents  $L_t^{-1}$  in Eq. (16) of [9] is written as

$$L_t^{-1} = \frac{1}{L_0^2} \begin{pmatrix} L_{11} & & 0 & M_1 & & 0 \\ & \ddots & & & \ddots & \\ 0 & & L_{1M} & 0 & & M_M \\ M_1 & & 0 & L_{12} & & 0 \\ & \ddots & & & \ddots & \\ 0 & & M_M & 0 & & L_{M2} \end{pmatrix} \quad (11)$$

where  $M_j = \sqrt{L_{j1}L_{j2} - L_0^2}$  with  $L_0 > 0$  being a small parameter giving the deviation from the tight coupling limit. We have

$$\mathcal{G} = \begin{pmatrix} 0 \\ 1_{2M \times 2M} \end{pmatrix} \quad (12)$$

and

$$M_0 = \mathcal{G} L_t^{-1} \mathcal{G}^t \quad (13)$$

$$= \begin{pmatrix} 0 & 0 \\ 0 & L_t^{-1} \end{pmatrix} \quad (14)$$

We construct a rotation matrix  $U$

$$U = \begin{pmatrix} 1 & 0 & & \cdots & & 0 \\ 0 & \frac{1}{\sqrt{1+t_1^2}} & & 0 & \frac{t_1}{\sqrt{1+t_1^2}} & 0 \\ & & \ddots & & & \\ \vdots & 0 & & \frac{1}{\sqrt{1+t_M^2}} & 0 & \frac{t_M}{\sqrt{1+t_M^2}} \\ & -\frac{t_1}{\sqrt{1+t_1^2}} & & 0 & \frac{1}{\sqrt{1+t_1^2}} & 0 \\ & & \ddots & & & \\ 0 & 0 & & -\frac{t_M}{\sqrt{1+t_M^2}} & 0 & \frac{1}{\sqrt{1+t_M^2}} \end{pmatrix} \quad (15)$$

where  $t_j = \sqrt{\frac{L_{j1}}{L_{j2}}}$ . We now compute  $U^t M_0 U$  and truncate it to its upper-left  $(M+1) \times (M+1)$  sector (by taking  $L_0 \rightarrow 0$  limit) which corresponds to the eigenspace with finite(non-infinite) eigenvalues. After truncation we get

$$M'_0 = \begin{pmatrix} 0 & 0 & & \\ & 1/L_1 & & \\ & & \ddots & \\ & 0 & & 1/L_M \end{pmatrix} \quad (16)$$

where  $L_j = L_{j1} + L_{j2}$ . After transforming  $C_0$  by computing  $U^t C_0 U$  and truncating we get  $C'_0$ . The matrix  $C'_0$  is in general non-zero in all its entries but below we construct a second transformation matrix  $T$  to make both  $C'_0$  and  $M'_0$  band-diagonal

$$T = \begin{pmatrix} 1 & & & 0 \\ -\frac{\sqrt{1+t_1^2}}{1-t_1} & -\frac{\sqrt{1+t_1^2}}{1-t_1} & & \\ & \frac{\sqrt{1+t_2^2}}{1-t_2} & \frac{\sqrt{1+t_2^2}}{1-t_2} & \\ & & \ddots & \ddots \\ 0 & & & (-1)^M \frac{\sqrt{1+t_M^2}}{1-t_M} & (-1)^M \frac{\sqrt{1+t_M^2}}{1-t_M} \end{pmatrix} \quad (17)$$

Applying  $T$  to  $C'_0$  and  $M'_0$  we get

$$C = T^t C'_0 T \quad (18)$$

$$= \begin{pmatrix} C_J + C'_1 & t_1 C'_1 & & 0 \\ t_1 C'_1 & t_1^2 C'_1 + C'_2 & \ddots & \\ & \ddots & \ddots & \\ 0 & & & t_{M-1}^2 C'_{M-1} + C'_M & t_M C'_M \\ & & & t_M C'_M & t_M^2 C'_M + C'_{M+1} \end{pmatrix} \quad (19)$$

$$M_0 = T^t M'_0 T \quad (20)$$

$$= \begin{pmatrix} \frac{1}{L'_1} & \frac{1}{L'_1} & & 0 \\ \frac{1}{L'_1} & \frac{1}{L'_1} + \frac{1}{L'_2} & \frac{1}{L'_2} & \\ & \frac{1}{L'_2} & \frac{1}{L'_2} + \frac{1}{L'_3} & \ddots \\ & & \ddots & \ddots \\ 0 & & & \frac{1}{L'_{M-1}} + \frac{1}{L'_M} & \frac{1}{L'_M} \\ & & & \frac{1}{L'_M} & \frac{1}{L'_M} \end{pmatrix} \quad (21)$$

where  $C'_j = C_j / (1 - t_j)^2$ ,  $L'_j = L_{j2} (1 - t_j)^2$ .

A Lagrangian  $\mathcal{L}_0$  (and equivalently a Hamiltonian  $\mathcal{H}_S$ ) can be written as

$$\mathcal{L}_0 = \frac{1}{2} \dot{\Phi}^T C \dot{\Phi} - U(\Phi), \quad \mathcal{H}_S = \frac{1}{2} Q^T C^{-1} Q + U(\Phi) \quad (22)$$

where

$$U(\Phi) = - \left( \frac{\Phi_0}{2\pi} \right)^2 L_J^{-1} \cos(\varphi_J) + \frac{1}{2} \Phi^T M_0 \Phi \quad (23)$$

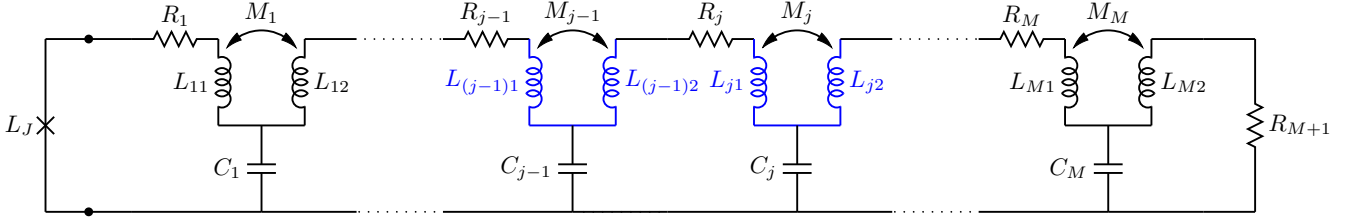


Figure 8: The  $j^{\text{th}}$  mode  $\Phi_j$  in Eq. (22) of the Brune circuit.  $\Phi_j$  is a linear combination of four branch fluxes  $\Phi_{j-1,1}, \Phi_{j-1,2}, \Phi_{j1}, \Phi_{j2}$  across inductors over two consecutive stages, as given by Eq. (29).

$\Phi$  is the vector of transformed (and truncated) coordinates of length  $(M+1)$ .  $\varphi_L$  is the phase across the Josephson junction. One can relate  $\Phi$  to the original branch fluxes in the Brune circuit by introducing an auxiliary vector  $\Phi'$  of length  $(M+1)$  and keeping track of two coordinate transformations  $U$  and  $T$  applied as follows

$$\Phi = T^t \Phi' \quad (24)$$

with

$$\Phi' = (\Phi_J, \Phi'_1, \dots, \Phi'_M) \quad (25)$$

$$= U^t (\Phi_J, \Phi_L)^t \quad (26)$$

where

$$(\Phi_J, \Phi_L) = (\Phi_J, \Phi_{12}, \Phi_{22}, \dots, \Phi_{M2}, \Phi_{11}, \Phi_{21}, \dots, \Phi_{M1}) \quad (27)$$

is the vector of fluxes of tree branches in the Brune circuit in Fig. 7,  $\Phi_J = \left(\frac{\Phi_0}{2\pi}\right) \varphi_J$  and  $\Phi'_j = \frac{1}{\sqrt{1+t_j^2}} (\Phi_{j2} - t_j \Phi_{j1})$ , for  $1 \leq j \leq M$ . Here we assume that the vector  $U^t (\Phi_J, \Phi_L)^t$  is truncated to its first  $(M+1)$  rows before assignment to  $\Phi'$ . As shown in Fig. 8 the mode  $\Phi_j$  of the circuit is a linear combination of four fluxes across inductors in stage  $j$  and  $j+1$ . More specifically we can write the  $j^{\text{th}}$  component of  $\Phi$  for  $2 \leq j \leq M$  by

$$\Phi_j = (-1)^{j-1} \frac{\sqrt{1+t_{j-1}^2}}{1-t_{j-1}} \Phi'_{j-1} + (-1)^j \frac{\sqrt{1+t_j^2}}{1-t_j} \Phi'_j \quad (28)$$

$$= \frac{(-1)^{j-1}}{1-t_{j-1}} (\Phi_{j-1,2} - t_{j-1} \Phi_{j-1,1}) + \frac{(-1)^j}{1-t_j} (\Phi_{j2} - t_j \Phi_{j1}) \quad (29)$$

For  $j=1, M+1$  we have  $\Phi_1 = \Phi_J - \frac{\sqrt{1+t_1^2}}{1-t_1} \Phi'_1 = \Phi_J - (\Phi_{12} - t_1 \Phi_{11}) / (1-t_1)$  and  $\Phi_{M+1} = (-1)^M \frac{\sqrt{1+t_M^2}}{1-t_M} \Phi'_M = (-1)^M (\Phi_{M2} - t_M \Phi_{M1}) / (1-t_M)$ , respectively. Note that the Josephson phase  $\Phi_J$  is given by  $\Phi_J = \sum_j (-1)^{j+1} \Phi_j$ .

To treat resistors in Caldeira-Leggett formalism we will first compute the dissipation matrix  $\mathcal{C}_Z(\omega)$  in Eq. (26) of [9]. We will then interpret the equation of motion  $(\mathcal{C} + \mathcal{C}_Z) * \ddot{\Phi} = -\frac{\partial U}{\partial \Phi}$  in Eq. (29) of [9] as an equation of motion Eq. (61) of [8] by taking the dissipative term to the right-hand side and writing (in frequency domain)  $\mathcal{C} \ddot{\Phi} = -\frac{\partial U}{\partial \Phi} - \omega^2 \mathcal{C}_Z \Phi$ . One can then relate  $\mathbf{M}_d(\omega) = \omega^2 \mathcal{C}_Z$  and  $K(\omega) = \omega^2 \bar{\mathcal{C}}_Z(\omega)$  where  $\mathbf{M}_d$  and  $K(\omega)$  are given in Eqs. (72-75) of [8]. Then coupling vectors  $\bar{\mathbf{m}}$  are identical in both formalisms.

We treat each resistor separately. Applying Eq. (124) of [8] we get the contribution to the relaxation rate from the resistor  $R_j$  ( $1 \leq j \leq M+1$ ):

$$\frac{1}{T_{1,j}} = 4 |\langle 0 | \bar{\mathbf{m}}_j \cdot \Phi | 1 \rangle|^2 J_j(\omega_{01}) \coth\left(\frac{\hbar\omega_{01}}{2k_B T}\right) \quad (30)$$

$|0, 1\rangle$  are the qubit eigenlevels of the system Hamiltonian Eq. (22). The vector  $\bar{\mathbf{m}}_j$  (of length  $(M+1)$ ) describes the coupling of the system to the environment representing resistor  $R_j$ . Note that our use of the non-normalized coupling

vector  $\bar{\mathbf{m}}_j$  and the flux vector  $\Phi$  implies removal of the factor  $\mu \left(\frac{\Phi_0}{2\pi}\right)^2$  from the definition of the spectral function of the bath  $J$  in Eq. (93) of [8] (See Eqs. (35) and (37) below).

For  $1 \leq j \leq M$ , using Eqs. (26-28) in [9] we compute

$$\bar{\mathbf{m}}_j = \begin{pmatrix} 0 \\ \vdots \\ 0 \\ \frac{(-1)^{j-1}C_j}{(1-t_j)} \\ \frac{(-1)^j C_{j+1}}{(1-t_{j+1})} + \frac{(-1)^{j-1} t_j C_j}{(1-t_j)} \\ \vdots \\ \frac{(-1)^{M-1} C_M}{(1-t_M)} + \frac{(-1)^{M-2} t_{M-1} C_{M-1}}{(1-t_{M-1})} \\ \frac{(-1)^{M-1} t_M C_M}{(1-t_M)} \end{pmatrix} \quad (31)$$

where  $\bar{\mathbf{m}}_j$  are vectors of length  $(M+1)$  and

$$\bar{\mathbf{C}}_{Z,j}(\omega) = -\frac{i\omega R_j}{1 + i\omega R_j \left( \sum_{k=j}^M C_k \right)} \quad (32)$$

We then have

$$K_j(\omega) = \omega^2 \bar{\mathbf{C}}_{Z,j}(\omega) \quad (33)$$

$$= \frac{i\omega^3 R_j}{1 + i\omega R_j \left( \sum_{k=j}^M C_k \right)} \quad (34)$$

Hence

$$J_j = \text{Im} [K_j(\omega)] \quad (35)$$

$$= \frac{\omega^3 R_j}{1 + \omega^2 R_j^2 \left( \sum_{k=j}^M C_k \right)^2} \quad (36)$$

To treat last resistor  $R_{M+1}$  we first replace  $C_{M+1}$  in the last row of capacitance matrix by  $1/(i\omega R_{M+1})$ . This gives a term  $-\frac{1}{R_{M+1}}\dot{\phi}_M$  on the right hand side of the equation of motion in Eq. (29) of [9]. This term can be treated with

[8]. It gives rise to a dissipation matrix  $\mathbf{M}_d = K_{M+1}(\omega) \bar{\mathbf{m}}_{M+1} \bar{\mathbf{m}}_{M+1}^T$  where  $K_{M+1}(\omega) = \frac{i\omega}{R_{M+1}}$  and  $\bar{\mathbf{m}}_{M+1} = \begin{pmatrix} 0 \\ \vdots \\ 0 \\ 1 \end{pmatrix}$

is a vector with  $(M+1)$  rows. We then have

$$J_{M+1}(\omega) = \text{Im} [K_{M+1}(\omega)] = \frac{\omega}{R_{M+1}} \quad (37)$$

### A. Degenerate case

As discussed in Appendix (III) Brune's algorithm may produce degenerate stages. In this text we will only consider the capacitive degenerate case. Such a case has appeared in the example circuit we studied as listed in Table II of the



$$\bar{\mathbf{m}}_a(j) = \begin{pmatrix} 0 \\ \vdots \\ 0 \\ j^{th} \text{ row} \longrightarrow (-1)^{j-1} \frac{C_j}{(1-t_j)} \\ (-1)^j \frac{C_{j+1}}{(1-t_{j+1})} + (-1)^{j-1} t_j \frac{C_j}{(1-t_j)} \\ \vdots \\ (-1)^{k-2} \frac{C_{k-1}}{(1-t_{k-1})} + (-1)^{k-3} t_{k-2} \frac{C_{k-2}}{(1-t_{k-2})} \\ k^{th} \text{ row} \longrightarrow (-1)^{k-2} t_{k-1} \frac{C_{k-1}}{(1-t_{k-1})} \\ 0 \\ \vdots \\ 0 \end{pmatrix} \quad (41)$$

$$\bar{\mathbf{m}}_b(j) = \begin{pmatrix} 0 \\ \vdots \\ 0 \\ (j-1)^{th} \text{ row} \longrightarrow (-1)^j \frac{C_j}{(1-t_j)} \\ (-1)^{j+1} \frac{C_{j+1}}{(1-t_{j+1})} + (-1)^j t_j \frac{C_j}{(1-t_j)} \\ \vdots \\ (-1)^M \frac{C_M}{(1-t_M)} + (-1)^{M-1} t_{M-1} \frac{C_{M-1}}{(1-t_{M-1})} \\ (-1)^M t_M \frac{C_M}{(1-t_M)} \end{pmatrix} \quad (42)$$

$$\bar{\mathbf{m}}_{C_k} = \left( 0 \ \cdots \ 0 \ C_k \ 0 \ \cdots \ 0 \right)^t \quad (43)$$

where  $C_k$  is in  $k^{th}$  row. Now we can write coupling vector  $\bar{\mathbf{m}}_j$  to the bath of the resistor  $R_j$  as a function of the vectors defined in Eqs. (41), (42), (43) above as

$$\bar{\mathbf{m}}_j = \begin{cases} \bar{\mathbf{m}}_a(j) + \bar{\mathbf{m}}_{C_k} + \bar{\mathbf{m}}_b(k) & \text{for } j < k \\ \bar{\mathbf{m}}_{C_k} + \bar{\mathbf{m}}_b(k) & \text{for } j = k \\ \bar{\mathbf{m}}_b(j) & \text{for } j > k \end{cases} \quad (44)$$

Note that vectors above are all of length  $M$ . Spectral densities  $J_i(\omega)$  are the same as in the non-degenerate case (Eqs. (35),(37)) for all resistors. Note also that dissipation treatment for the last resistor  $R_{M+1}$  is unaffected since  $C_{M+1}$  is untouched in Eq. (40).

### III. BRUNE'S METHOD

Brune extended[6] Foster's[3] work to lossy networks. He formulated necessary and sufficient conditions for a rational function  $Z(s)$  to correspond to a passive lumped element circuit including possibly resistors. He coined the term "positive real (PR)" for such functions. He also devised an algorithm to synthesize a circuit given a PR function  $Z(s)$ . Below we define PR property and describe Brune's algorithm. For more details see [5]. In the following we stick with the electrical engineering convention for the imaginary unit  $j = -i$ .

#### A. PR property

A scalar impedance function  $Z(s)$  is PR if the following two conditions are met

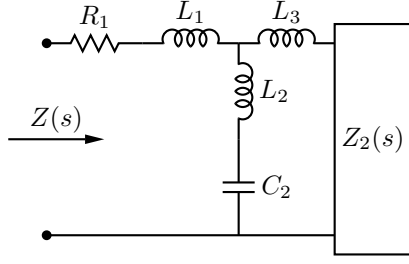


Figure 9: Brune circuit extraction step

- 1)  $Z(s)$  is a rational function which is real for real values of  $s$ .
- 2)  $\text{Re}[Z(s)] \geq 0$  for  $\text{Re}[s] \geq 0$ .

The second condition is equivalent to the following

- 1) No poles lie in the right half plane.
- 2) Poles on the  $j$ -axis have finite positive real residues and are simple.
- 3)  $\text{Re}[Z(j\omega)] \geq 0$ .

### B. Brune's algorithm

1. If  $Z(s)$  or  $Y(s) = 1/Z(s)$  has  $j$ -axis poles, remove them by realizing terms corresponding to those poles in the partial fraction expansion. Those terms correspond to parallel  $LC$  resonators (connected in series) in case of  $Z(s)$  poles and series  $LC$  resonators (connected in parallel) for  $Y(s)$  poles. Repeat until no  $j$ -axis pole is left.
2. Find  $\omega_1$  and  $R_1$  such that  $R_1 = \min_{\omega} Z(j\omega)$  and  $Z(j\omega_1) = R_1$ . Define  $Z_1(s) = Z(s) - R_1$ . This step corresponds to the removal of  $R_1$  in Fig. 9.
3. Define  $L_1 = Z_1(j\omega_1)/(j\omega_1)$ . If we extract the inductance  $L_1$  as shown in Fig. 9,  $1/(Z_1(s) - L_1s)$  is the admittance corresponding to the rest of the circuit and has a pole at  $s = j\omega_1$ , hence we can write

$$\frac{1}{Z_1(s) - L_1s} = \frac{(1/L_2)s}{s^2 + \omega_1^2} + \frac{1}{W(s)} \quad (45)$$

4. The first term in Eq. (45) corresponding to the pole at  $s = j\omega_1$  is realized with a shunt  $LC$  branch consisting of inductance  $L_2$  connected in series with capacitance  $C_2 = 1/(L_2\omega_1^2)$  as shown in Fig. 9.
5.  $W(s)$  has a pole at infinity such that

$$\lim_{s \rightarrow \infty} W(s) = -\frac{L_1L_2s}{L_1 + L_2} = L_3s \quad (46)$$

This pole is removed by constructing  $Z_2(s) = W(s) - L_3s$  which corresponds to connecting in series an inductance of value  $L_3 = -L_1L_2/(L_1 + L_2)$ .  $Z_2(s)$  is PR with no  $j$ -axis poles or zeros and whole process (steps 1 to 5) can now be applied to  $Z_2$ .

Steps 1 to 5 reduce degrees of both numerator and denominator of  $Z(s)$  by 2 so that the algorithm terminates once a constant  $Z_2(s) = R$  is reached.

The circuit in Fig. 9 potentially involves negative values for inductances  $L_1$  and  $L_3$  [5]. However one can replace the T-shaped inductive part of the circuit in Fig. 9 with a "tightly coupled" inductor as shown in Fig. 10 where the inductances are related by

$$L_{11} = L_1 + L_2 \quad (47)$$

$$L_{22} = L_3 + L_2 \quad (48)$$

$$M = L_2 \quad (49)$$

Note that lower terminals of the coupled inductor are short-circuited. A generic 2-port coupled inductor is shown in Fig. 11 with the following constitutive relations

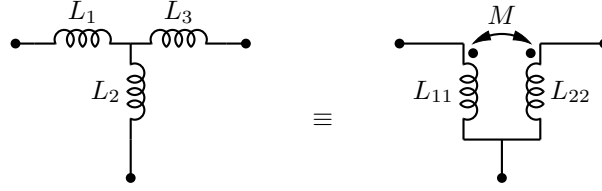


Figure 10: Equivalence of T-shaped inductive circuit in Fig. 9 to a coupled inductor

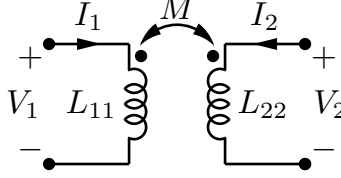


Figure 11: Generic 2-port coupled inductor with convention chosen for current directions and voltage polarities

$$\begin{pmatrix} \Phi_1 \\ \Phi_2 \end{pmatrix} = \begin{pmatrix} L_{11} & M \\ M & L_{22} \end{pmatrix} \begin{pmatrix} I_1 \\ I_2 \end{pmatrix} \quad (50)$$

assuming the conventions shown in Fig. 11 for current directions and voltage polarities. With the current directions chosen the stored energy in the coupled inductor is given by

$$E = \frac{1}{2} (L_{11}I_1 + 2MI_1I_2 + L_{22}I_2) \quad (51)$$

Note that in step (2) above one may find  $\omega_1 = 0$  or  $\omega_1 = \infty$ . In case of  $\omega_1 = \infty$  we have the degenerate circuit in Fig. 12 which corresponds to the circuit in Fig. 10 with  $L_1 = L_2 = L_3 = 0$ . This condition is equivalent to  $L'_k \rightarrow 0$  and  $t_k \rightarrow 0$ .  $C_j$  in Fig. 12 is given by

$$C_j = \lim_{s \rightarrow \infty} \frac{1}{s(Z_j - R_j)} \quad (52)$$

#### IV. LOSSY FOSTER METHOD

Foster's Theorem can be extended to responses with small loss [4]. We start with the partial fraction expansion for  $Z(s)$

$$Z(s) = \sum_k \frac{R_k}{s - s_k} \quad (53)$$

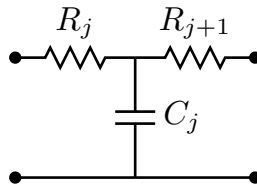


Figure 12: A degenerate stage in Brune circuit

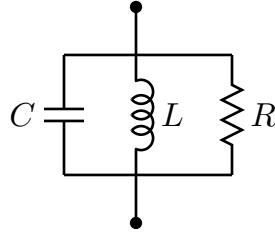


Figure 13: Generic shunt resonant stage in lossy Foster circuit

where  $R_k$ 's are residues and  $s_k$ 's are poles. Residues and poles come in complex conjugate pairs. If we define

$$s_k = \xi_k + j\omega_k \quad (54)$$

$$R_k = a_k + jb_k \quad (55)$$

Collecting terms corresponding to conjugate pairs

$$Z_k(s) = \frac{R_k}{s - s_k} + \frac{R_k^*}{s - s_k^*} = 2 \frac{a_k s - (a_k \xi_k + b_k \omega_k)}{s^2 - 2\xi_k s + \xi_k^2 + \omega_k^2} \quad (56)$$

One can show that for physical circuits with small loss  $\xi_k$  and  $b_k$  are both small quantities [5]. Hence we can approximately write

$$Z_k(s) \cong \frac{2a_k s}{s^2 - 2\xi_k s + \omega_k^2} \quad (57)$$

The impedance function of the shunt-resonant circuit as depicted in Fig. 13 is

$$Z(s) = \frac{\frac{\omega_0 R}{Q} s}{s^2 + \frac{\omega_0}{Q} s + \omega_0^2} \quad (58)$$

with

$$\omega_0^2 = \frac{1}{LC} \quad (59)$$

$$Q = \omega_0 RC \quad (60)$$

Hence we see that we can realize the function  $Z_k(s)$  in Eq. (57) by a circuit as in Fig. 13 with

$$R = -a_k/\xi_k \quad (61)$$

$$\omega_0 = \omega_k \quad (62)$$

$$Q = -\omega_k/2\xi_k \quad (63)$$

and the impedance in Eq. (53) can be realized as in Fig. 14 by a series connection of stages in Fig. 13.

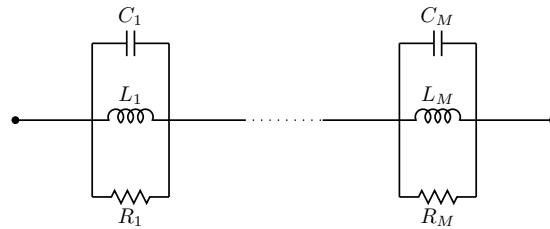


Figure 14: Lossy Foster Circuit